REVIEW

Contributions of Raman spectroscopy to the understanding of bone strength

Gurjit S Mandair and Michael D Morris

Department of Chemistry, University of Michigan, Ann Arbor, MI, USA.

Raman spectroscopy is increasingly commonly used to understand how changes in bone composition and structure influence tissue-level bone mechanical properties. The spectroscopic technique provides information on bone mineral and matrix collagen components and on the effects of various matrix proteins on bone material properties as well. The Raman spectrum of bone not only contains information on bone mineral crystallinity that is related to bone hardness but also provides information on the orientation of mineral crystallites with respect to the collagen fibril axis. Indirect information on collagen cross-links is also available and will be discussed. After a short introduction to bone Raman spectroscopic parameters and collection methodologies, advances in *in vivo* Raman spectroscopic measurements for animal and human subject studies will be reviewed. A discussion on the effects of aging, osteogenesis imperfecta, osteoporosis and therapeutic agents on bone composition and mechanical properties will be highlighted, including genetic mouse models in which structure–function and exercise effects are explored. Similarly, extracellular matrix proteins, proteases and transcriptional proteins implicated in the regulation of bone material properties will be reviewed.

Introduction

Raman spectroscopy has become an important tool in the assessment of bone quality, because the technique can be used with fresh, as well as fixed and imbedded, specimens and, with limitations, can be used for noninvasive measurements on live animals. The sampling versatility must be balanced against a lower signal/noise ratio than that obtained in bone Fourier transform infrared (FTIR) spectroscopy, which provides much the same information. Although there have been a few scattered reports of noninvasive acquisition of bone Raman spectra of human subjects, there have been no validation studies to date.

The Bone Raman Spectrum

Figure 1 shows a typical Raman spectrum of bone. The major mineral and matrix bands are summarized in **Table 1**. Many assignments are taken from Penel *et al.*,[1] with references to other sources in which more recent work has required modification of the assignments. Bone matrix band assignments are mostly those of collagen type I. Most spectra are reported only for a window from about 400 cm^{-1} to about 1750 cm^{-1}. This region includes characteristic bands of bone mineral and bone matrix, but it does not include matrix C–H and N–H stretches.

These are found in the 2900–3300 cm^{-1} region. With few exceptions, these bands contain little information that is not available in lower wavenumber bands.
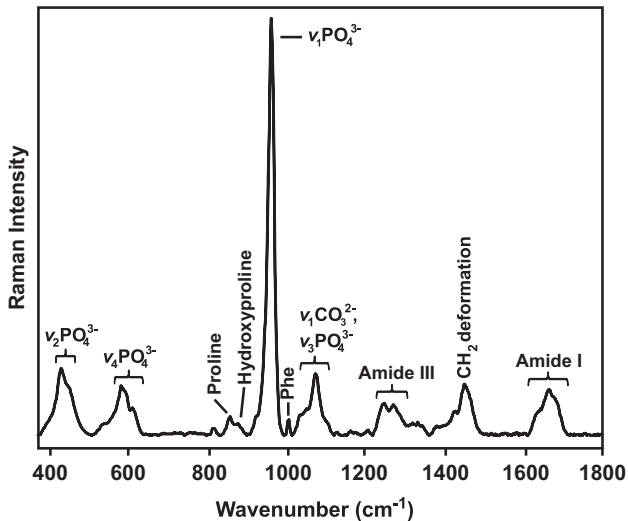
Mineral bands that are intense in Raman spectra will be weak in FTIR spectra, and vice versa. However, although relative intensities may be different, most matrix bands in the Raman spectra are the same as in the FTIR spectra. Major exceptions are a prominent phenylalanine band in the Raman spectrum (1003 cm^{-1}) that is weak or absent in the FTIR spectra and the prominent amide II in FTIR spectra (1540–1580 cm^{-1}) that is absent in the Raman spectra[2] (nonspecialist introductions to the theory of Raman spectroscopy are available for those who wish to explore the physical chemistry underlying the general rules governing relative intensities).[3,4]

There is some variability in the reported position of major bands. In part, the variability is real and is a function of age, health status and of differences among human subjects and among the rodent animal models used. However, there may also be small 1–2 cm^{-1} systematic errors from instrument drift or miscalibration. Changes of band position from some reference state such as an age point or before administration of a chemical agent or an exercise protocol are usually unaffected if the spectroscopy system is stable over the measurement period. Reported band intensity ratios may also be affected if

Correspondence: Dr MD Morris, Department of Chemistry, University of Michigan, 930 N University Avenue, Ann Arbor, MI 48109 1055, USA.
E-mail: mdmorris@umich.edu

the detector is not calibrated for the wavelength dependence of its response or if the analysis does not account for the presence of one or more weak and unresolved bands. Comparison of direct and peak-fitting methods has been reported for some bands in bone Raman and FTIR spectra.[5]

The most widely used mineral band is a phosphate band at $\sim 959\,cm^{-1}$ ($\nu_1 PO_4^{3-}$), which is characteristic of carbonated apatites. The exact position is sensitive to mineral carbonate (CO_3^{2-}) and monohydrogen phosphate (HPO_4^{2-}) content. Newly deposited mineral has a high HPO_4^{2-} content that shifts this band to a lower wavenumber.[6–8] The full-width half-height of the $\nu_1 PO_4^{3-}$ band is inversely proportional to mineral crystallite c-axis length, and it is often used as a measure of mineral crystallinity. The most intense B-type carbonate band at $1070\,cm^{-1}$ ($\nu_1 CO_3^{2-}$) for bone mineral lies close to a component of a phosphate band at $1076\,cm^{-1}$ ($\nu_3 PO_4^{3-}$), and accurate measurement requires careful band fitting.[9]

The most widely reported collagen band is amide I. The band is actually a composite of several partially resolved components. The most important bands are at $1660\,cm^{-1}$ and $1690\,cm^{-1}$. Using FTIR spectroscopy, the ratio of these two components was shown to be proportional to the relative amounts of the trivalent cross-link pyridinoline and the divalent (immature) cross-link dihydroxylysinonorleucine.[10] This ratio was soon imported into Raman spectroscopy, and ratio changes were used as evidence for rupture of cross-links caused by mechanical indentation of bone.[11] By extension, increases in the $1660/1690\,cm^{-1}$ intensity ratio has been used to infer the presence of pathological cross-links, as discussed in later sections.

Figure 1 Baselined-corrected Raman spectrum of mouse cortical bone acquired using a 785-nm laser. Major bone mineral and matrix collagen band positions and associated spectral regions are marked.

Table 1 Raman spectroscopic band assignments for bone mineral and matrix components

Raman shift, cm^{-1}	Assignment	Comments	Reference(s)
430	$\nu_2 PO_4^{3-}$	Strong band	[1]
450	$\nu_2 PO_4^{3-}$	Shoulder on 430 cm^{-1} band	[1]
584–590	$\nu_4 PO_4^{3-}$	Multiple partially resolved components	[1]
609	$\nu_4 PO_4^{3-}$	Shoulder on 590 cm^{-1} band	[1]
668	$\nu(C–S)$	Cysteine	[1,85]
756	$\nu_4 CO_3^{2-}$	B-type carbonate, very weak	[1]
853	$\nu(C–C)$	Collagen proline, may include $\delta(C–C–H)$ contribution from tyrosine	[1,85]
872	$\nu(C–C)$	Mostly collagen hydroxyproline	[61,86]
920	$\nu(C–C)$	Shoulder, mostly collagen proline	[86,87]
937	$\nu(C–C)$	Proline and protein backbone	[1,85]
955	$\nu_1 PO_4^{3-}$	Transient bone mineral (P–O) phase, usually seen in immature bone.	[6]
957	$\nu_1 PO_4^{3-}$	Bone mineral containing extensive HPO_4^{2-}, usually immature	[6]
959–962	$\nu_1 PO_4^{3-}$	Bone mineral, mature	[1,6,9]
1003	$\nu(C–C)$	Phenylalanine	[1,87]
1035	$\nu_3 PO_4^{3-}$	Overlaps with proline $\nu(C–C)$ component	[9,86]
1048	$\nu_3 PO_4^{3-}$		[1,9]
1060	Proteoglycan	Overlaps with lipids, collagen and components of $\nu_3 PO_4^{3-}$	[88]
1070	$\nu_1 CO_3^{2-}$	Overlaps with component of $\nu_3 PO_4^{3-}$	[9]
1076	$\nu_3 PO_4^{3-}$	Overlaps with component of $\nu_1 CO_3^{2-}$	[9]
1176	$\nu(C–O–C)$	Tyrosine, phenylalanine	[1,85]
1204	$\omega(CH_2)$	Tyrosine, hydroxyproline	[85,86]
1242	Amide III	Protein β-sheet and random coils	[85,89]
1272	Amide III	Protein α-helix	[85]
1293–1305	$\delta(=CH)$	Lipid band, sometimes seen in fresh untreated bone	[1,90]
1340	Amide III	Protein α-helix, sometimes called CH_2CH_2 wag	[1,85]
1365	Pentosidine	Overlap with lipid 1369 cm^{-1} band	[1,12,13,85]
1375	Proteoglycan	Representative of glycosaminoglycans	[88]
1446	$\delta(CH_2)$	Protein CH_2 deformation	[1,85]
1585	$\nu(C–C–H)$	Weak band, aromatic ring	[1]
1609	$\delta(C=C)$	Phenylalanine, tyrosine	[85]
1640	$\nu(C=C)$	Shoulder to 1660 cm^{-1} band	[1,61]
1660	Amide I	Strongest amide I $\nu(C=O)$ component, polarization sensitive	[1,17]
1690	Amide I	Shoulder, prominent with immature cross-links The band also relates to β-sheet or disordered secondary structure	[45,51,91]

Amide I components are measures of changes in collagen secondary structure, rather than direct measures of collagen cross-link content. Few collagen cross-links are sufficiently abundant to have directly observable Raman markers. An exception is a band at 1362 cm^{-1}, which has been assigned to advanced glycation end products in a rat model of chronic kidney disease.[12,13] Unsurprisingly, the interpretation of the 1660/1690 cm^{-1} intensity ratio has been contentious, leading some to call it the matrix maturity ratio.[14] The ratio does depend on measurement conditions, especially if agents such as β-aminopropionitrile that perturb cross-linking are used.[15]

Absolute measurements of Raman band intensities are difficult, especially in turbid media such as bone. For this reason, Raman metrics are usually band intensity ratios. They include the mineral/matrix ratio, carbonate/phosphate ratio and the collagen cross-link (or collagen maturity) ratio. The major exception is crystallinity, which is usually measured as the inverse of the phosphate 959 cm^{-1} band width. In many cases, the choice of a mineral or matrix band does not matter, except that more intense bands will provide more precise results.

However, in confocal Raman microscopy, polarization effects can influence band intensities.[16] The problem can be minimized by using a randomly polarized (also called unpolarized) laser or by using bands that are polarization-insensitive (called depolarized in the Raman literature).[17,18] Both phosphate $\nu_1 PO_4^{3-}$ and collagen amide I bands are strongly polarization-dependent. Polarization effects in microspectroscopy are minimized with low numerical aperture objectives and, if available, slit spatial filters rather than pinhole spatial filters in the microscope.[19]

Although the phosphate 959 cm^{-1} band is almost universally accepted as a measure of bone mineral content, there is disagreement over the band to use as a measure of matrix content. Candidates include amide I (1660 cm^{-1}), amide III (1242 cm^{-1}), CH_2 deformation (1446 cm^{-1}), phenylalanine (1003 cm^{-1}) and proline (853 cm^{-1}) or proline + hydroxyproline (853 + 876 cm^{-1}). Several groups object to the use of most of these bands because they are not collagen-specific. The proline or proline + hydroxyproline markers do not have this problem.

There are a few validation studies. A few band intensity ratios have been correlated with corresponding FTIR ratios.[5,20] Recently, the $\nu_2 PO_4^{3-}$/amide III intensity ratio has been shown to be proportional to calcium content, as measured by quantitative backscattered electron microscopy, with correction for the different sampling properties of electron microscopy and optical microscopy.[21]

Experimental

Most instruments use near-infrared (NIR) lasers to minimize tissue fluorescence. The most commonly used wavelength is 785 nm. At this excitation wavelength, C–H stretches are visible, but N–H stretches are found at wavelengths beyond the long wavelength response limit of most currently available detectors. Spectrographs are usually operated with a resolution of at least 8 cm^{-1} to avoid instrument-induced band-broadening effects. Low-noise charged-coupled device detectors are used to capture bands in a wide window (usually about 2000 cm^{-1}) of Raman shifts simultaneously.

Microprobes

Most commercially available Raman microprobes are built around standard research microscope frames, to which the vendor adds the excitation laser and the spectrograph/detector components, as well as supporting software. In many recent instruments, the microscope stage and other light-sensitive parts of the system are in a light-tight enclosure to enable measurements in room light.

Fiber optic probes

There is increasing use of fiber optic probes for bone Raman spectroscopy. Most probes are compact and can be used at distances of several meters from the instrument. Some are designed to contact a specimen, whereas others are non-contact and rely on lenses to deliver laser light and collect Raman scatter. The topic has been reviewed by Sato et al.[22]

The simplest probe design uses a single optical fiber to transmit laser light and collect backscattered Raman signal. A dichroic filter or other optic is used to separate the exciting laser beam and signal. The distal end of the fiber may be lensed to control the depth of penetration or to allow noncontact operation. In a closely related design, the beams from separate excitation and collection fibers are combined near their distal ends, and a single lens is used for excitation and collection.

The second basic design, generally called an N-around-1, has a single excitation fiber surrounded by one or two rings of collection fibers.[23] This configuration provides efficient collection of scattered light. Dielectric filters may be used at or near the distal end to remove silica Raman scatter from the excitation fiber and to prevent backscattered laser light from entering the collection fibers and generating silica background.

A related fiber optic probe design enables noninvasive bone Raman spectroscopy, although only at limited depths below the skin. Human and animal tissues are highly scattering, and probing more than a millimeter below the surface requires that the laser light injection and collection of Raman scatter be spatially separated.[24] The technique is called diffuse spectroscopy in the tissue fluorescence and NIR absorption literatures and spatially offset Raman spectroscopy (SORS) in the Raman literature.[25] The N-around-1 design was shown to have subsurface probing capability in the mid-1990s.[26] The implications for depth penetration were not fully realized until a decade later when the first versatile probe designs were demonstrated and the theory was developed.[24]

In vivo SORS has been demonstrated in mice,[27,28] and the results have been validated against measurements made on excised bone.[27] Recently, the first in vivo human subject SORS has been reported.[29] The measurement site was the tibial plateau. Although validation by direct measurement of bone of the volunteer was impossible, the data agreed well with periosteal tibial Raman spectra from cadaveric tissue. Because of light scattering, the depth of penetration in backscattered mode is limited to less than 1 cm in human subjects or animals.

Diffuse Raman tomography is based on the spatial offset principle.[30–32] The methodology is the same as for diffuse fluorescence and NIR absorbance diffuse tomography.[33] Unlike the more familiar X-ray micro-computed tomography (micro-CT) or magnetic resonance imaging, elastic light scattering (turbidity) limits the amount of detail available. Best results are obtained when the optical spectroscopic

data are fitted to a model based on a high-resolution tomography, such as micro-CT.

Although most investigators have used principal components analysis-based methods to extract Raman spectra from sets of transcutaneous measurements, fitting to a library of bone components and soft tissue components works well, especially for the mineral/matrix ratio.[34] If band fitting is used, it is advisable to use the second derivative technique or an equivalent method to determine the number of bands in the fit.[10,35]

Calibration

Calibration of the wavelength/wavenumber and intensity axes of the Raman system is important for inter-laboratory comparisons and to correct for instrument drift, but investigators do not always report calibration protocols. For wavelength calibration, the gold standard is a rare gas atomic discharge lamp, usually a neon lamp, using wavelength values measured by the US National Institute of Standards and Technology (NIST) (http://www.nist.gov/pml/data/asd.cfm). An excellent alternative is one or more standard materials specified by American Society for Testing and Materials (ASTM) International.[36] They are stable chemical compounds whose consensus Raman spectra are given in the standard. The intensity axis can be calibrated against the output from a stabilized and calibrated quartz-halogen lamp. A simpler alternative is the fluorescence from a NIST standard Raman reference glass.[37] For bone Raman spectroscopy at 785-nm excitation, the recommended glass is NIST SRM 2241.[38]

Development and Aging Effects

An early study of intramembranous mineralization using parietal sections from murine skulls ranging from 13-day embryos (before mineralization) to 6-month-old (skeletally mature) animals found that Raman signatures of mineral varied with skeletal development.[39] Force-induced craniosynostosis was shown to be a rate effect only, with mineral that was indistinguishable from normal bone mineral.[40] Mineral development has been studied using cranial tissue section cultures sampled every 12 h[6] and, more recently, hourly.[8] Hourly interrogation allows observation of circadian mineralization periodicity and its temporal relation to peripheral clock gene expression. Increasing crystallinity (decrease in the $\nu_1PO_4^{3-}$ band width) is aperiodic and reaches a c-axis length limit of about 22 nm, as determined by correlation of band width against powder X-ray spectroscopy.

In male human cortical bone, skeletal mineralization and mineral carbonation increases and crystallinity decreases, and the variance about the means of these parameters decreases with age, indicating that the overall tissue composition becomes increasingly homogeneous with age.[41] In female femoral head specimens, bone near an osteoporotic fracture was found to be less mineralized but with more highly carbonated mineral than bone 2 mm from the fracture site.[42] The carbonate/amide I ratio was the only significant differentiator between undamaged bone of fractured specimens and undamaged controls. It is not clear why phosphate/amide I was not a significant predictor, although this may be a function of the high variability of this ratio in the fracture specimens. Confounding factors include possible damage to tissue 2 mm from the fracture, as well as small specimen sizes. However, the same study also found that in iliac crest biopsies, in cortical bone but not in trabecular bone, carbonate/phosphate ratio was significantly higher in fracture victims than in controls. This and other early studies of B-type carbonation may be compromised by the presence of a nearby component of $\nu_3PO_4^{3-}$, because the Raman spectrum in that region was not fully elucidated until 2007.[9]

Correlation with Biomechanical Parameters

There are discrepancies in the literature correlating Raman spectroscopic parameters and biomechanical parameters. Confounding factors include choice of tissue (rodent versus human), age (chronological age versus time of deposition), anatomic site, whether cortical or trabecular bone was tested and whether measurements are of periosteal surface or an average across a cross-section. Still, general patterns are observable.

In an early study of female Sprague–Dawley rats of ages 3–24 months, stiffness and bending modulus were found to be significantly dependent on crystallinity, degree of mineralization and B-type carbonate content.[43] Yield stress was found to be significantly dependent on crystallinity and degree of mineralization. Follow-up work on human cadaveric specimens of femoral cortical tissue confirmed mineral composition effects on modulus, yield stress and fracture stress, and also showed positional effects.[44] In a more detailed mouse model study of age effects, it was shown that the most important Raman spectroscopic predictors of mechanical properties varied with animal age.[45] It has been shown in a mouse model that Raman composition parameters correlate with mechanical properties at the whole bone (3-point bending) and tissue level (nanoindentation).[46]

Animal Age Effects

Although animal age has usually been the subject of Raman spectroscopic studies, tissue age presents a very different picture. Hardness and indentation modulus appear to be independent of mineral/matrix and carbonate/phosphate ratios until substantial amounts of mineral are laid down, although the authors fit their entire data set to straight lines.[47]

There are a few studies of the correlation between biomechanical parameters and Raman spectroscopic composition parameters in mouse models of disorders, including osteogenesis imperfect (OI)[48–51] and osteoporosis,[52] as well as on the effects of knocking out matrix proteinase,[53] transcription factor[54] and noncollagenous proteins.[55–62] These are discussed in the following sections.

Osteogenesis Imperfecta

There have been surprisingly few applications of Raman spectroscopy to the study of OI. Most mouse model studies have used either oim/oim or Brtl/+. The heterozygous Brtl/+ has cysteine in place of glycine at position 349 on one COL1(a1) chain, and it is a model for OI type IV. In oim/oim mice, the matrix trimeric COL1(a1)$_3$ rather than COL1(a1)$_2$(a2). As a model for OI is oim/oim is largely obsolete, but it is widely used in biophysical and other studies on defective matrix.

Early on, Brtl/+ was reported to have differences in mineral/matrix and carbonate/phosphate ratios at 2 and 6 months,

compared with wild type, although most were not statistically significant.[48] This model has demonstrated that that use of alendronate to speed fracture healing has no significant effect on existing bone or the callus boundary 3 weeks post fracture, whereas reduced crystallinity and increased carbonate/phosphate ratio imply some incipient increase in mineralization.[50] Oim/oim mouse has been used to demonstrate composition differences between male and female mice,[49] increased disorder of collagen and mineral by polarized Raman[19] and noninvasive measurements by time-resolved Raman spectroscopy[63] and SORS.[34]

Recent work with tissue from human OI patients has confirmed increased mineral/matrix ratio, decreased crystallinity and both a shift in amide I wavenumber and a decrease in amide I intensity, itself consistent with increased mineral/matrix ratio.[64] At the mouse model level, transplantation of human fetal blood stem cells into oim/oim during gestation shows partial rescue of mechanical properties, as well as spectroscopic differences between wild-type, treated and untreated mice.[65] Similar results have been shown for grafting bone marrow into Brtl/+. Mutations in gene *FKBP10*, which codes for FKBP65, a collagen chaperone, cause a decrease in collagen cross-linking, detectable by Raman spectroscopy.[62] The decrease is directly because of reduced hydroxylation of proline.

Osteoporosis, Models and Treatment Effects

Several studies have shown that Raman spectroscopy can detect compositional changes in osteoporotic bone following bisphosphonate and/or parathyroid hormone treatment.[66–68] Some model and treatment studies have gone further to examine relationships between changes in osteoporotic bone composition with alternations in bone material properties.[52,69–72] For example, the mineral/matrix ratio and indentation modulus were found to be reduced in cancellous bone from the lumbar spine of female donors with osteoporosis.[71] In another study, femurs from SAMP6 mice had impaired failure properties that were partially attributed to reduced collagen content and reduced collagen/mineral ratios, as determined by collagen biochemical analysis and Raman spectroscopy, respectively.[52]

In regard to treatment effects, femurs from osteoporotic sheep treated with zoledronate (ZOL) or raloxifene (RAL) were examined using colocalized Raman microscopy and nanoindentation techniques, including lamellar aligned collagen measurements obtained by second harmonic generation microscopy.[69] Carbonate substitution, crystallinity and lamellar aligned collagen parameters explained the greatest variability in indentation modulus and hardness following RAL treatment. In contrast, mineral/matrix ratio, crystallinity and/or lamellar aligned collagen parameters only partially explained the variability in hardness following ZOL treatment. Other contributors to bone composition, such as nonenzymatic collagen cross-links, mineral crystal orientation and noncollageneous proteins may also need to be considered.

Glucocorticoid Effects

Raman maps of trabecular bone acquired from glucocorticoid (GC)-administered mice showed that mineral/matrix ratios surrounding osteocyte lacunae were reduced and that the reductions were associated with changes in elastic modulus.[73]

In another study related to rheumatoid arthritis, tibiae from GC-administered wild-type mice not only exhibited reduced mineral/matrix ratios but also exhibited increased carbonate/phosphate and collagen cross-link ratios compared with wild-type placebo controls.[74] Increases in cross-link ratios were consistent with changes in bone biomechanical properties found in this study.

TGF-β Signaling Effects

In a study of genetically modified mice with altered transforming growth factor-β (TGF-β) levels, an inverse relationship between TGF-β signaling and bone mechanical properties was found.[75] Bone from *Smad3*$^{+/-}$ mice, in which TFG-β expression was impaired, exhibited the highest bone mineral concentration, elastic modulus and hardness compared with *D4* mice, the phenotype with the highest TFG-β expression. Elastic modulus mapping studies revealed considerable heterogeneity of bone matrix in *D4* mice and which was spatially correlated with Raman maps of matrix or mineral components. These results and more recent findings suggest that the pharmacological reduction of TGF-β expression may improve bone material properties, especially in patients with bone cancer.[76]

In a study of femurs from mice in which TGF-β expression was inhibited by a 1D11 antibody, the bending strength and tissue-level modulus were increased. Mineral/collagen ratios of trabecular bone were also increased, whereas carbonate/phosphate and crystallinity levels were unchanged, indicating that 1D11 treatment did not impair the purity of hydroxyapatite.[77]

Vitamin D Deficiency Effects

In the study of material properties of femurs in growing rats, dietary deficiency in vitamin D resulted in reduced Raman mineral/matrix ratio, which was consistent with reduced bone mineralization measurements made by micro-CT.[78] A moderate relationship between tissue modulus and Raman mineral/matrix ratio was also found. However, the relationship was bimodal, possibly indicating changes in bone tissue mechanical requirements during primary and secondary mineralization. Similar reductions in mineral/matrix ratios had been reported in humeri from rats following dietary intervention. However, the results were only significant for whole bone FTIR and not tissue-level Raman spectroscopic measurements.[79]

A recent synchrotron radiation micro-CT (SRμCT) study found that the bone hidden underneath the osteoid layer in osteomalacic bone continued to mineralize unabated.[80] Raman spectroscopy and FTIR found evidence for altered collagen secondary structure and changes in collagen maturity/mineral composition, respectively, that were consistent with aged bone. *In situ* toughness tests and 3D SRμCT imaging revealed greater numbers of initiation and propagation cracks in osteomalacic bone. These results supported the hypothesis that osteoclasts could not penetrate the thick undermineralized osteoid layer in osteomalacic bone, whereas mineral outside the osteoid frame was subject to remodeling.

Inbred and Knockout Mouse Models

Structure–function studies have shown that inbred A/J mice have smaller femoral diameters, larger cortical thicknesses and higher mineral/matrix ratios than B6 mice.[81] A/J femora were

also found to be mechanically robust in terms of stiffness, but their higher mineral content made them more brittle than B6 femora. Correlations between mineral/matrix ratios and elastic modulus (loading, unloading), yield strength and hardness were also highlighted in this study.

To relate genetic traits with responsiveness to mechanical stimuli, exercised and nonexercised B6;129 and C3H mice were studied.[58] Mineral/matrix, carbonate/phosphate and collagen cross-links ratios were all increased in C3H mice, whereas exercised B6;129 mice had higher carbonate/phosphate ratios, post-yield deformation and failure deformation. These results showed that mechanical stimuli could influence bone material properties and that it was strain-specific. Although increased collagen cross-links ratios failed to elicit changes in C3H mice bone mechanical properties, they could have maintained the mechanical integrity of bone by mitigating tissue rearrangement. Exercised and nonexercised biglycan-deficient B6;129 and C3H mice were also examined in this study and compared against their wild-type counterparts.

By examining bones from $Mmp2^{-/-}$ and $Mmp9^{-/-}$ mice, differential effects of deleting MMP-2 and MMP-9 on bone architecture, composition and material properties could be determined.[53] For instance, the deletion of MMP-2 reduced tibial mineral/matrix ratio that was consistent with lower tissue-level modulus and hardness relative to controls. In contrast, deletion of MMP-9 reduced trabecular tissue mineral density (TMD) and thickness relative to controls. Taken together, the loss of MMP-2 disrupted tissue-level mechanical properties, whereas loss of MMP-9 affected bone architecture. In a follow-up study, correlations between bone compositional parameters and whole bone and tissue-level mechanical properties were examined, including those with cortical TMD.[46]

The role of phospho1 in maintaining bone quality and strength in $Phospho1^{-/-}$ knockout mice has been recently reported.[82] $Phospho1^{-/-}$ long bones deformed plastically during 3-point bending tests, whereas the majority of long bones from wild-type mice fractured. The deformability of $Phospho1^{-/-}$ bone was attributed to the low bone mineralization status and young age of the mice. Moreover, tissue-level modulus and hardness were compromised in $Phospho1^{-/-}$ mice. With Raman spectroscopy, $Phospho1^{-/-}$ bone had lower mineral/matrix and carbonate/phosphate ratios. Overall, the loss of phospho1 resulted in undermineralized, immature bone that was able to deform without fracturing.

The involvement of the activating transcription factor 4 (ATF4) in bone development has been established using Atf4-deficient mice.[83] To clarify the role of ATF4 on the resistance of bone to fracture, intact femurs and embedded tibial cross-sections from $Atf4^{-/-}$ and $Atf4^{+/+}$ male mice were examined.[54] No significant difference was evident in either the material strength or cortical TMD in femurs from $Atf4^{-/-}$ and $Atf4^{+/+}$ mice. However, femurs from 20-week $Atf4^{-/-}$ mice had higher mineral/collagen ratios and were more brittle with lower fracture toughness than $Atf4^{+/+}$ mice. By using the polarization-sensitive mineral/amide I parameter, $Atf4^{+/+}$ mice exhibited more fibril anisotropy, suggesting that bone matrix contributed to the brittleness phenotype.

Femurs from fibrillin-2 ($Fbn2^{-/-}$),[55] fetuin-A/alpha-HS-glycoprotein ($Ahsg^{-/-}$),[59] osteopontin ($OPN^{-/-}$)[56] and osteocalcin ($OC^{-/-}$)[57]-deficient mice have been studied using bone mechanics and Raman spectroscopy. In one study, $Fbn2^{-/-}$ mice had decreased hardness and elastic modulus in the midcortical region and decreased carbonate/phosphate ratio in the endosteal region relative to wild-type controls.[55] This study showed that Fbn2 deficiency directly influenced the mechanical properties of bone. However, a recent FTIR imaging study indicates that Fbn1-deficiency has a far greater role than Fbn2 in regulating the material properties of bone.[84] In contrast, despite $Ahsg^{-/-}$ mice having stunted femoral bones and increased cortical thickness, no significant differences in bone material properties, mineral/matrix ratios or collagen fibril orientation were found when compared with the wild-type genotype.[59] These results show that Fetuin-A/$Ahsg$ has a greater developmental, rather than structural, role in this model.

Osteopontin (OPN) has a critical role in the early stages of mineralization, because the loss of OPN resulted in young mice with reduced cortical hardness and elastic modulus relative to age-matched $OPN^{+/+}$ and older $OPN^{-/-}$ mice (>12 weeks).[56] Moreover, mineral/matrix ratios were lower in younger $OPN^{-/-}$ mice. Raman spectroscopic studies on the $OC^{-/-}$ genotype suggest that OC also has a role in mineralization, but unlike in the $OPN^{-/-}$ genotype mineral/matrix ratios were not different between $OC^{-/-}$ and $OC^{+/+}$ mice.[57] In contrast, $OC^{-/-}$ mice have lower carbonate/phosphate ratios and reduced crystallinity than $OC^{+/+}$ mice. This suggests that OC regulates the growth of apatitic crystals, which was consistent with nanoindentation studies in which tissue hardness increased more than elastic modulus in $OC^{-/-}$ mice.

The depletion of osteoblast-derived bone morphogenic protein-2 (BMP2) could cause structural and mechanical defects in long bones of Osx-Cre knockout mice, but Raman spectroscopic analyses could not explain these defects.[60] The authors suggested that other parameters related to collagen alignment, cross-links and structure should be examined. In another study, Raman spectroscopy found that calvarial osteoblastic cell cultures treated with BMP2 in the presence or absence of lysyl oxidase resulted in mineralized tissue with distinct collagen secondary structures[61] Moreover, BMP2 and lysyl oxidase treatment yielded $in vitro$ mineralized tissue with increased hardness and elastic modulus, which were comparable to that of 4-week-old calvarial bone.

Conflict of Interest

The authors declare no conflict of interest.

Acknowledgements

References

1. Penel G, Delfosse C, Descamps M, Leroy G. Composition of bone and apatitic biomaterials as revealed by intravital Raman microspectroscopy. *Bone* 2005;**36**:893–901.
2. Morris MD, Finney WF. Recent developments in Raman and infrared spectroscopy and imaging of bone tissue. *Spectroscopy* 2004;**18**:155–159.
3. Smith E, Dent G. *Modern Raman Spectroscopy: A Practical Approach*. John Wiley & Sons: Chichester, United Kingdom, 2005.
4. Sasic S, Ozaki Y. *Raman, Infrared, and near-Infrared Chemical Imaging*. John Wiley & Sons: Hoboken, NJ, USA, 2010.

5. Turunen MJ, Saarakkala S, Rieppo L, Helminen HJ, Jurvelin JS, Isaksson H. Comparison between infrared and raman spectroscopic analysis of maturing rabbit cortical bone. *Appl Spectrosc* 2011;**65**:595–603.

6. Crane NJ, Popescu V, Morris MD, Steenhuis P, Ignelzi MA Jr . Raman spectroscopic evidence for octacalcium phosphate and other transient mineral species deposited during intra-membranous mineralization. *Bone* 2006;**39**:434–442.

7. Kazanci M, Fratzl P, Klaushofer K, Paschalis EP. Complementary information on *in vitro* conversion of amorphous (precursor) calcium phosphate to hydroxyapatite from raman microspectroscopy and wide-angle X-ray scattering. *Calcif Tissue Int* 2006;**79**:354–359.

8. McElderry J-DP, Zhao G, Khmaladze A, Wilson CG, Franceschi RT, Morris MD. Tracking circadian rhythms of bone mineral deposition in murine calvarial organ cultures. *J Bone Miner Res* 2013;**28**:1846–1854.

9. Awonusi A, Morris MD, Tecklenburg MMJ. Carbonate assignment and calibration in the raman spectrum of apatite. *Calcif Tissue Int* 2007;**81**:46–52.

10. Paschalis EP, Verdelis K, Doty SB, Boskey AL, Mendelsohn R, Yamauchi M. Spectroscopic characterization of collagen cross-links in bone. *J Bone Miner Res* 2001;**16**:1821–1828.

11. Carden A, Rajachar RM, Morris MD, Kohn DH. Ultrastructural changes accompanying the mechanical deformation of bone tissue: A Raman imaging study. *Calcif Tissue Int* 2003;**72**:166–175.

12. Iwasaki Y, Kazama JJ, Yamato H, Fukagawa M. Changes in chemical composition of cortical bone associated with bone fragility in rat model with chronic kidney disease. *Bone* 2011;**48**:1260–1267.

13. Iwasaki Y, Kazama JJ, Yamato H, Shimoda H, Fukagawa M. Accumulated uremic toxins attenuate bone mechanical properties in rats with chronic kidney disease. *Bone* 2013;**57**:477–483.

14. Farlay D, Duclos M-E, Gineyts E, Bertholon C, Viguet-Carrin S, Nallala J *et al.* The ratio 1660/1690 cm-1 measured by Infrared microspectroscopy is not specific of enzymatic collagen cross-links in bone tissue. *PLoS One* 2011;**6**:e28736.

15. Paschalis EP, Tatakis DN, Robins S, Fratzl P, Manjubala I, Zoehrer R *et al.* Lathyrism-induced alterations in collagen cross-links influence the mechanical properties of bone material without affecting the mineral. *Bone* 2011;**49**:1232–1241.

16. Kazanci M, Roschger P, Paschalis EP, Klaushofer K, Fratzl P. Bone osteonal tissues by Raman spectral mapping: Orientation-composition. *J Struct Biol* 2006;**156**:489–496.

17. Makowski AJ, Patil CA, Mahadevan-Jansen A, Nyman JS. Polarization control of Raman spectroscopy optimizes the assessment of bone tissue. *J Biomed Opt* 2013;**18**:55005.

18. Gamsjaeger S, Masic A, Roschger P, Kazanci M, Dunlop JWC, Klaushofer K *et al.* Cortical bone composition and orientation as a function of animal and tissue age in mice by Raman spectroscopy. *Bone* 2010;**47**:392–399.

19. Raghavan M, Sahar ND, Wilson RH, Mycek M-A, Pleshko N, Kohn DH *et al.* Quantitative polarized Raman spectroscopy in highly turbid bone tissue. *J Biomed Opt* 2010;**15**:037001.

20. Gourion-Arsiquaud S, Burket JC, Havill LM, DiCarlo E, Doty SB, Mendelsohn R *et al.* Spatial variation in osteonal bone properties relative to tissue and animal age. *J Bone Miner Res* 2009;**24**:1271–1281.

21. Roschger A, Gamsjaeger S, Hofstetter B, Masic A, Blouin S, Messmer P *et al.* Relationship between the v2PO4/amide III ratio assessed by Raman spectroscopy and the calcium content measured by quantitative backscattered electron microscopy in healthy human osteonal bone. *J Biomed Opt* 2014;**19**:065002.

22. Sato H, Shinzawa H, Komachi Y. Fiber-optic Raman probes for biomedical and pharmaceutical applications. In: Matousek P, Morris MD (eds) *Emerging Raman Applications and Techniques in Biomedical and Pharmaceutical Fields.* Springer: Berlin Heidelberg, 2010, p 25–45.

23. Utzinger U, Richards-Kortum RR. Fiber optic probes for biomedical optical spectroscopy. *J Biomed Opt* 2003;**8**:121–147.

24. Matousek P, Stone N. Recent advances in the development of Raman spectroscopy for deep non-invasive medical diagnosis. *J Biophotonics* 2013;**6**:7–19.

25. Matousek P, Clark IP, Draper ERC, Morris MD, Goodship AE, Everall N *et al.* Subsurface probing in diffusely scattering media using spatially offset Raman spectroscopy. *Appl Spectrosc* 2005;**59**:393–400.

26. Cooney TF, Skinner HT, Angel SM. Comparative study of some fiber-optic remote Raman probe designs. Part II: Tests of single-fiber, lensed, and flat- and bevel-tip multi-fiber probes. *Appl Spectrosc* 1996;**50**:849–860.

27. Schulmerich MV, Cole JH, Kreider JM, Esmonde-White F, Dooley KA, Goldstein SA *et al.* Transcutaneous Raman spectroscopy of murine bone *in vivo. Appl Spectrosc* 2009;**63**:286–295.

28. Peterson JR, Okagbare PI, De La Rosa S, Cilwa KE, Perosky JE, Eboda ON *et al.* Early detection of burn induced heterotopic ossification using transcutaneous Raman spectroscopy. *Bone* 2013;**54**:28–34.

29. Buckley K, Kerns JG, Parker AW, Goodship AE, Matousek P. Decomposition of *in vivo* spatially offset Raman spectroscopy data using multivariate analysis techniques. *J Raman Spectrosc* 2014;**45**:188–192.

30. Srinivasan S, Schulmerich M, Cole JH, Dooley KA, Kreider JM, Pogue BW *et al.* Image-guided Raman spectroscopic recovery of canine cortical bone contrast in situ. *Opt Express* 2008;**16**:12190–12200.

31. Schulmerich MV, Cole JH, Dooley KA, Morris MD, Kreider JM, Goldstein SA *et al.* Noninvasive Raman tomographic imaging of canine bone tissue. *J Biomed Opt* 2008;**13**:020506.

32. Demers J-LH, Davis SC, Pogue BW, Morris MD. Multichannel diffuse optical Raman tomography for bone characterization *in vivo*: a phantom study. *Biomed Opt Express* 2012;**3**:2299–2305.

33. Jacques SL, Pogue BW. Tutorial on diffuse light transport. *J Biomed Opt* 2008;**13**: 041302–041319.

34. Maher JR, Inzana JA, Awad HA, Berger AJ. Overconstrained library-based fitting method reveals age- and disease-related differences in transcutaneous Raman spectra of murine bones. *J Biomed Opt* 2013;**18**:077001.

35. Adams MJ. *Chemometrics in Analytical Spectroscopy.* The Royal Society of Chemistry: Cambridge, United Kingdom, 1995.

36. International A. *E1840-96. Standard Guide for Raman Shift Standards for Spectrometer Calculation West Conshohocken.* ASTM International: West Conshohocken, PA, USA, 2007, p11.

37. International A. *E2911-13 Standard Guide for Relative Intensity Correction of Raman Spectrometers.* ASTM International: West Conshohocken, PA, USA, 2013, p12.

38. Rae A, Stosch R, Klapetek P, Hight Walker AR, Roy D. State of the art Raman techniques for biological applications. *Methods* 2014;**68**:338–347.

39. Tarnowski CP, Ignelzi MA, Morris MD. Mineralization of developing mouse calvaria as revealed by Raman microspectroscopy. *J Bone Miner Res* 2002;**17**:1118–1126.

40. Tarnowski CP, Ignelzi MA, Wang W, Taboas JM, Goldstein SA, Morris MD. Earliest mineral and matrix changes in force-induced musculoskeletal disease as revealed by Raman micro-spectroscopic imaging. *J Bone Miner Res* 2004;**19**:64–71.

41. Yerramshetty JS, Lind C, Akkus O. The compositional and physicochemical homogeneity of male femoral cortex increases after the sixth decade. *Bone* 2006;**39**:1236–1243.

42. McCreadie BR, Morris MD, Chen T-c, Rao DS, Finney WF, Widjaja E *et al.* Bone tissue compositional differences in women with and without osteoporotic fracture. *Bone* 2006;**39**:1190–1195.

43. Akkus O, Adar F, Schaffler MB. Age-related changes in physicochemical properties of mineral crystals are related to impaired mechanical function of cortical bone. *Bone* 2004;**34**:443–453.

44. Yerramshetty JS, Akkus O. The associations between mineral crystallinity and the mechanical properties of human cortical bone. *Bone* 2008;**42**:476–482.

45. Raghavan M, Sahar ND, Kohn DH, Morris MD. Age-specific profiles of tissue-level composition and mechanical properties in murine cortical bone. *Bone* 2012;**50**:942–953.

46. Bi X, Patil CA, Lynch CC, Pharr GM, Mahadevan-Jansen A, Nyman JS. Raman and mechanical properties correlate at whole bone- and tissue-levels in a genetic mouse model. *J Biomech* 2011;**44**:297–303.

47. Donnelly E, Boskey AL, Baker SP, van der Meulen MCH. Effects of tissue age on bone tissue material composition and nanomechanical properties in the rat cortex. *J Biomed Mater Res A* 2010;**92**(3):1048–1056.

48. Kozloff KM, Carden A, Bergwitz C, Forlino A, Uveges TE, Morris MD *et al.* Brittle IV mouse model for osteogenesis imperfecta IV demonstrates postpubertal adaptations to improve whole bone strength. *J Bone Miner Res* 2004;**19**:614–622.

49. Yao XM, Carleton SM, Kettle AD, Melander J, Phillips CL, Wang Y. Gender-dependence of bone structure and properties in adult osteogenesis imperfecta murine model. *Ann Biomed Eng* 2013;**41**:1139–1149.

50. Meganck JA, Begun DL, McElderry JD, Swick A, Kozloff KM, Goldstein SA *et al.* Fracture healing with alendronate treatment in the Brtl/ plus mouse model of osteogenesis imperfecta. *Bone* 2013;**56**:204–212.

51. Bart ZR, Hammond MA, Wallace JM. Multi-scale analysis of bone chemistry, morphology and mechanics in the oim model of osteogenesis imperfecta. *Connect Tissue Res* 2014;**55**:4–8.

52. Silva MJ, Brodt MD, Wopenka B, Thomopoulos S, Williams D, Wassen MHM *et al.* Decreased collagen organization and content are associated with reduced strength of demineralized and intact bone in the SAMP6 mouse. *J Bone Miner Res* 2006;**21**:78–88.

53. Nyman JS, Lynch CC, Perrien DS, Thiolloy S, O'Quinn EC, Patil CA *et al.* Differential effects between the loss of MMP-2 and MMP-9 on structural and tissue-level properties of bone. *J Bone Miner Res* 2011;**26**:1252–1260.

54. Makowski AJ, Uppuganti S, Wadeer SA, Whitehead JM, Rowland BJ, Granke M *et al.* The loss of activating transcription factor 4 (ATF4) reduces bone toughness and fracture toughness. *Bone* 2014;**62**:1–9.

55. Kavukcuoglu NB, Arteaga-Solis E, Lee-Arteaga S, Ramirez F, Mann AB. Nanomechanics and Raman spectroscopy of fibrillin 2 knock-out mouse bones. *J Mater Sci* 2007;**42**:8788–8794.

56. Kavukcuoglu NB, Denhardt DT, Guzelsu N, Mann AB. Osteopontin deficiency and aging on nanomechanics of mouse bone. *J Biomed Mater Res A* 2007;**83**(1):136–144.

57. Kavukcuoglu NB, Patterson-Buckendahl P, Mann AB. Effect of osteocalcin deficiency on the nanomechanics and chemistry of mouse bones. *J Mech Behav Biomed Mater* 2009;**2**: 348–354.

58. Wallace JM, Golcuk K, Morris MD, Kohn DH. Inbred strain-specific effects of exercise in wild type and biglycan deficient mice. *Ann Biomed Eng* 2010;**38**:1607–1617.

59. Seto J, Busse B, Gupta HS, Schafer C, Krauss S, Dunlop JWC *et al.* Accelerated growth plate mineralization and foreshortened proximal limb bones in Fetuin-A knockout mice. *PLoS One* 2012;**7**:e47338.

60. McBride SH, McKenzie JA, Bedrick BS, Kuhlmann P, Pasteris JD, Rosen V *et al.* Long bone structure and strength depend on BMP2 from osteoblasts and osteocytes, but not vascular endothelial cells. *PLoS One* 2014;**9**:e96862.

61. Shibata Y, Suzuki D, Wurihan, Yamada A, Maruyama N, Fujisawa N *et al.* Lysyl oxidase like-2 reinforces unsatisfactory ossification induced by bone morphogenetic protein-2: Relating nanomechanical properties and molecular changes. *Nanomedicine* 2013;**9**:1036–1047.

62. Barnes AM, Cabral WA, Weis M, Makareeva E, Mertz EL, Leikin S *et al.* Absence of FKBP10 in recessive type XI osteogenesis imperfecta leads to diminished collagen cross-linking and reduced collagen deposition in extracellular matrix. *Hum Mutat* 2012;**33**:1589–1598.

63. Draper ERC, Morris MD, Camacho NP, Matousek P, Towrie M, Parker AW *et al.* Novel assessment of bone using time-resolved transcutaneous Raman spectroscopy. *J Bone Miner Res* 2005;**20**:1968–1972.

64. Imbert L, Auregan J-C, Pernelle K, Hoc T. Mechanical and mineral properties of osteogenesis imperfecta human bones at the tissue level. *Bone* 2014;**65**:18–24.

65. Vanleene M, Saldanha Z, Cloyd KL, Jell G, Bou-Gharios G, Bassett JHD *et al.* Transplantation of human fetal blood stem cells in the osteogenesis imperfecta mouse leads to improvement in multiscale tissue properties. *Blood* 2011;**117**:1053–1060.

66. Gamsjaeger S, Hofstetter B, Zwettler E, Recker R, Gasser JA, Eriksen EF *et al.* Effects of 3 years treatment with once-yearly zoledronic acid on the kinetics of bone matrix maturation in osteoporotic patients. *Osteoporos Int* 2013;**24**:339–347.

67. Olejnik C, Falgayrac G, During A, Vieillard MH, Maes JM, Cortet B *et al.* Molecular alterations of bone quality in sequesters of bisphosphonates-related osteonecrosis of the jaws. *Osteoporos Int* 2014;**25**:747–756.

68. Gamsjaeger S, Buchinger B, Zoehrer R, Phipps R, Klaushofer K, Paschalis EP. Effects of one year daily teriparatide treatment on trabecular bone material properties in postmenopausal osteoporotic women previously treated with alendronate or risedronate. *Bone* 2011;**49**:1160–1165.

69. Burket JC, Brooks DJ, MacLeay JM, Baker SP, Boskey AL, van der Meulen MCH. Variations in nanomechanical properties and tissue composition within trabeculae from an ovine model of osteoporosis and treatment. *Bone* 2013;**52**:326–336.

70. Matsumoto Y, Mikuni-Takagaki Y, Kozai Y, Miyagawa K, Naruse K, Wakao H *et al.* Prior treatment with vitamin K-2 significantly improves the efficacy of risedronate. *Osteoporos Int* 2009;**20**:1863–1872.

71. Kim G, Cole JH, Boskey AL, Baker SP, van der Meulen MCH. Reduced tissue-level stiffness and mineralization in osteoporotic cancellous bone. *Calcif Tissue Int* 2014;**95**:125–131.

72. Miyagawa K, Kozai Y, Ito Y, Furuhama T, Naruse K, Nonaka K *et al.* A novel underuse model shows that inactivity but not ovariectomy determines the deteriorated material properties and geometry of cortical bone in the tibia of adult rats. *J Bone Miner Metab* 2011;**29**:422–436.

73. Lane NE, Yao W, Balooch M, Nalla RK, Balooch G, Habelitz S *et al.* Glucocorticoid-treated mice have localized changes in trabecular bone material properties and osteocyte lacunar size that are not observed in placebo-treated or estrogen-deficient mice. *J Bone Miner Res* 2006;**21**:466–476.

74. Takahata M, Maher JR, Juneja SC, Inzana J, Xing L, Schwarz EM *et al.* Mechanisms of bone fragility in a mouse model of glucocorticoid-treated rheumatoid arthritis Implications for insufficiency fracture risk. *Arthritis Rheum* 2012;**64**:3649–3659.

75. Balooch G, Balooch M, Nalla RK, Schilling S, Filvaroff EH, Marshall GW *et al.* TGF-beta regulates the mechanical properties and composition of bone matrix. *Proc Natl Acad Sci USA* 2005;**102**:18813–18818.

76. Buijs JT, Stayrook KR, Guise TA. The role of TGF-beta in bone metastasis: novel therapeutic perspectives. *Bonekey Rep* 2012;**1**:96–96.

77. Edwards JR, Nyman JS, Lwin ST, Moore MM, Esparza J, O'Quinn EC *et al.* Inhibition of TGF-beta signaling by 1D11 antibody treatment increases bone mass and quality *in vivo*. *J Bone Miner Res* 2010;**25**:2419–2426.

78. Kim G, Boskey AL, Baker SP, van der Meulen MCH. Improved prediction of rat cortical bone mechanical behavior using composite beam theory to integrate tissue level properties. *J Biomech* 2012;**45**:2784–2790.

79. Donnelly E, Chen DX, Boskey AL, Baker SP, van der Meulen MCH. Contribution of mineral to bone structural behavior and tissue mechanical properties. *Calcif Tissue Int* 2010;**87**:450–460.

80. Busse B, Bale HA, Zimmermann EA, Panganiban B, Barth HD, Carriero A *et al.* Vitamin D deficiency induces early signs of aging in human bone, increasing the risk of fracture. *Sci Transl Med* 2013;**5**:193ra88.

81. Pathak S, Vachhani SJ, Jepsen KJ, Goldman HM, Kalidindi SR. Assessment of lamellar level properties in mouse bone utilizing a novel spherical nanoindentation data analysis method. *J Mech Behav Biomed Mater* 2012;**13**:102–117.

82. Huesa C, Yadav MC, Finnila MAJ, Goodyear SR, Robins SP, Tanner KE *et al.* PHOSPHO1 is essential for mechanically competent mineralization and the avoidance of spontaneous fractures. *Bone* 2011;**48**:1066–1074.

83. Yang XG, Matsuda K, Bialek P, Jacquot S, Masuoka HC, Schinke T *et al.* ATF4 is a substrate of RSK2 and an essential regulator of osteoblast biology: Implication for Coffin-Lowry syndrome. *Cell* 2004;**117**:387–398.

84. Arteaga-Solis E, Sui-Arteaga L, Kim M, Schaffler MB, Jepsen KJ, Pleshko N *et al.* Material and mechanical properties of bones deficient for fibrillin-1 or fibrillin-2 microfibrils. *Matrix Biol* 2011;**30**:188–194.

85. Movasaghi Z, Rehman S, Rehman IU. Raman spectroscopy of biological tissues. *Appl Spectrosc Rev* 2007;**42**:493–541.

86. Frushour BG, Koenig JL. Raman-scattering of collagen, gelatin, and elastin. *Biopolymers* 1975;**14**:379–391.

87. Wopenka B, Kent A, Pasteris JD, Yoon Y, Thomopoulos S. The tendon-to-bone transition of the rotator cuff: A preliminary Raman spectroscopic study documenting the gradual mineralization across the Insertion in rat tissue samples. *Appl Spectrosc* 2008;**62**:1285–1294.

88. Gamsjaeger S, Klaushofer K, Paschalis EP. Raman analysis of proteoglycans simultaneously in bone and cartilage. *J Raman Spectrosc* 2014;**45**:794–800.

89. Dehring KA, Crane NJ, Smukler AR, McHugh JB, Roessler BJ, Morris MD. Identifying chemical changes in subchondral bone taken from murine knee joints using Raman spectroscopy. *Appl Spectrosc* 2006;**60**:1134–1141.

90. Lakshmi RJ, Alexander M, Kurien J, Mahato KK, Kartha VB. Osteoradionecrosis (ORN) of the mandible: A laser Raman spectroscopic study. *Appl Spectrosc* 2003;**57**:1100–1116.

91. Takahata M, Maher JR, Juneja SC, Inzana J, Xing L, Schwarz EM *et al.* Mechanisms of bone fragility in a mouse model of glucocorticoid-treated rheumatoid arthritis Implications for insufficiency fracture risk. *Arthritis Rheum* 2012;**64**:3649–3659.